Semiconductor laser coupled to a finite-response time phase-conjugate mirror

David H. DeTienne
George R. Gray

Department of Electrical Engineering, University of Utah

Govind P. Agrawal

The Institute of Optics, University of Rochester

Daan Lenstra

Department of Physics and Astronomy, Free University, Amsterdam.

ABSTRACT

Most of the previous treatments of semiconductor lasers subject to optical feedback from a phase-conjugate mirror (PCM) have assumed the PCM responds instantaneously. Furthermore, the mechanism responsible for phase conjugation does not usually enter into the analysis. In this paper are derived the time-dependent reflectivity from a PCM created through non-degenerate four-wave mixing. The resulting laser dynamics are compared to the case of the ideal PCM, as a function of PCM mirror interaction depth, distance to the PCM, and laser current. The time-responsive PCM tends to suppress otherwise chaotic output and produces power pulses whose frequency is tunable by varying laser current or PCM reflectivity.

Keywords: semiconductor laser, optical feedback, chaos, chaos control, pulses, tunable frequency

1. INTRODUCTION

The effects of optical feedback from phase-conjugate reflectors has been attracting considerable attention lately, due in part to the potential for creating ultrashort, mode-locked pulses.[1,2,3,4,5,6] Semiconductor lasers subject to PCF exhibit behavior which can differ radically from the effects of COF. Some of these differences were reviewed for the case of a single-longitudinal mode semiconductor laser.[7] When the semiconductor laser oscillates in multiple longitudinal modes, PCF obtained through four wave mixing can lead to mode locking and short-pulse output.[1]

The theoretical modeling has generally assumed for simplicity that the phase-conjugate mirror (PCM) responds instantaneously to the incident radiation. This assumption may often be too restrictive experimentally, for example when the PCM is constructed from a Barium-Titanate crystal or from an atomic vapor. Furthermore, the physical mechanism responsible for the PCM,

generally four-wave mixing, is usually ignored in the simulations. The purpose of this paper is to correct the above-mentioned deficiencies and to demonstrate the resulting dynamics of a laser subject to feedback resulting from such a PCM. In particular, we show that such PCF can lead to tunable frequency pulsed output, even though the laser current is constant.

2. MODELING

Earlier efforts to model PCF were done by simple modification of the model for COF. This led to a limiting case, however. A conventional mirror has a relatively flat spectral response, fast response time, and a thin interaction depth. A phase conjugate mirror, by contrast, tends to have a peaked frequency response, a finite interaction depth (hence the appellation "deep PCF"), and may respond sluggishly. In this work we develop an improved model for PCF, and show some interesting results from simulations. Fig. 1 shows the experimental diagram and parameters of interest.

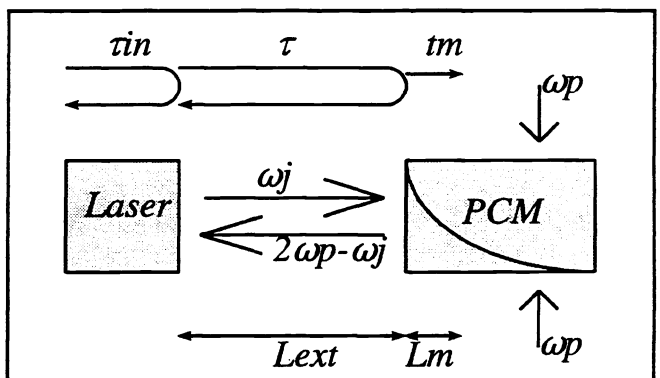

Figure 1 Experiment schematic showing equation parameters.

For an instantaneously responding PCM, the simplest rate equations for a semiconductor laser subject to PCF are:

$$\frac{dN}{dt} = \frac{I}{q} - \frac{N}{\tau_e} - G|E|^2 \tag{1}$$

$$\frac{dE}{dt} = \frac{1}{2}(1 - i\alpha)(G-\gamma)E(t) + \kappa E^*(t-\tau) \tag{2}$$

In Eqs. 1 and 2, N is the carrier number of the laser, I is the current, q the electron charge, and τ_e is the carrier lifetime. E is the laser's complex electric field at the output facet. α is the linewidth enhancement factor, ($\alpha = 3$). G is the gain which depends linearly on the carrier number N, and γ is the loss. κ is the feedback rate, a measure of the reflectivity of the phase-conjugate mirror (PCM). The PCF term, as in the case of ordinary feedback, depends on the field at one round trip earlier, time τ. In contrast to COF, however, the field is conjugated by the PCM. The equations are integrated in the weak-feedback regime, so multiple round trip reflections could be safely neglected. The laser is assumed to operate in just one longitudinal mode. The results shown in this paper are deterministic in nature, since no random-noise terms are included.

Eq. 2 shows the idealized case where the feedback comes from an instantaneously

responding PCM. The conjugated feedback term, $E^*(t-\tau)$, gives the feedback from just one round trip time τ earlier. The starting point for a better PCF model is the standard expression for the frequency-dependent reflectivity due to non-degenerate four wave mixing, given by Eqs. 3 and 4:[8]

$$r_{pcm}(\omega) = \frac{-i\,\kappa_c \tan(\beta L_m)}{\beta - (i\Delta k/2)\tan(\beta L_m)} \tag{3}$$

$$\Delta k = \frac{2(\omega - \omega_p)(\epsilon_0 \epsilon_r)^2}{c} \tag{4}$$

where κ_c and β are proportional to $\chi^{(3)}$ and the pump E fields, and are functions of the frequency mismatch between the pump and signal beams. L_m is the penetration depth, Δk is the wave-number mismatch between the pump frequency ω and ω_p, ω_p is the frequency of peak response for the PCM, ϵ_0 is the permittivity of free space, ϵ_r is the relative permittivity (index of refraction $n = \sqrt{\epsilon_r}$), and c is the speed of light. The equations are simplified if a parameter t_m in Eq. 5 is defined. t_m is approximately the time it takes the light to penetrate the PCM. With this definition, the phase conjugate reflectivity simplifies to Eq. 6.

$$t_m = \frac{n \tan(\beta L_m)}{\beta c} \cong \frac{n L_m}{c} \tag{5}$$

$$r_{pcm}(\omega) = \frac{\kappa_c c}{n} \frac{t_m}{t_m(\omega - \omega_p) + i} \tag{6}$$

Eqs. 3 and 6 for the phase-conjugate reflectivity assume a monochromatic probe beam. Since even a single-longitudinal mode semiconductor laser can have a linewidth as large as 100 MHz, we need to integrate $r_{pcm}(\omega)$ over the probe laser linewidth. This can be expressed as a Fourier integral, so that the phase-conjugate field becomes:

$$E_{pc} = \int_{-\infty}^{+\infty} r_{pcm}(\omega)\, A^*(\omega - \omega_0)\, e^{-i(\omega-\omega_0)(t-\tau)} d\omega \tag{7}$$

where A is the Fourier component of the probe, and ω_0 is the center frequency of the pump beam. By doing a contour integration of this integral and applying the residue theorem, Eq. 8 results:

$$E_{pc} = \int_{-\infty}^{t} E^*(t'-\tau)\, e^{-\frac{(1-i\delta_0 t_m)(t-t')}{t_m}} dt' \tag{8}$$

where δ_0 is the detuning between the monochromatic pump beam and the center frequency of the probe, set to zero for this paper. Applying these results leads to the improvement of Eq. 2, the original laser rate equation, to Eq. 9:

$$\frac{dE}{dt} = \frac{1}{2}(1 - i\alpha)(G-\gamma)E(t) + \frac{i\kappa}{t_m}\int_{-\infty}^{t} E^*(t'-\tau)\, e^{-\frac{(t-t')}{t_m}}\, dt' \qquad (9)$$

Numerically, Eq. 9 is very inefficient to apply directly. That would require numerically solving the feedback integral each numerical integration time step. Moreover, separating Eq. 9 into two separate equations, the standard method for reducing higher order differential equations into a system of first order equations, leads to a numerical instability. Fortunately, we were able to come up with a recursive definition for the feedback integral:

$$E_{pc}(t) = E^*\left(t-\frac{\Delta t}{2}-\tau\right) e^{-\frac{\Delta t}{2t_m}}\Delta t + e^{-\frac{\Delta t}{t_m}} E_{pc}(t-\Delta t) \qquad (10)$$

where Δt is the size of an numerical integration time step. The first term is a rectangle approximation for the most recent Δt of the E_{pc} integral (Eq. 8), and the second term recursively gives everything previous.

3. DEEP PCF SIMULATION RESULTS

3.1 Overview

With a simulated system, the parameter space that can be searched is huge, as any element in the equations can be varied. Physically, many parameters cannot by varied by turning a knob in the laboratory (the value of α, for instance). We chose to vary the depth of the PCM (t_m, which can be varied by choice of PCM, physical size, or diameters of the pump beams[9]); the field reflectivity of the PCM (r_3); the external cavity length (L_{ext}); and the laser current (I/I_{th}). All of these parameters can be varied experimentally.

An important tool for searching the parameter space is the bifurcation diagram. The bifurcation diagrams tell at a glance the state of the system for a range of bifurcation variable values. Where there are no bifurcation points, the system is stable. Where a single line exists the system is period one, i.e. just one dominant frequency. Where there are two lines the system is period two, etc. A filled-in area indicates very high order periodicity or chaos.[10]

3.2 Depth of the PCM

First, we investigate the effect of PCM depth by changing the parameter t_m. Thus we can see how our improved rate equations differ from those of the usually-assumed ideal PCM. These simulations were made with a current ratio of $I/I_{th} = 1.05$, and external cavity spacing $L_{ext} = 10$ cm. Fig. 2 shows a bifurcation diagram, with reflectivity as the bifurcation variable, for the instantaneous PCM, that is $t_m = 0.0$ ns. Also shown in Fig. 2 are the average power and the standard deviation of the power. There is a one-to-one correspondence between the chaotic regions in the bifurcation diagram and a large standard deviation, as expected.

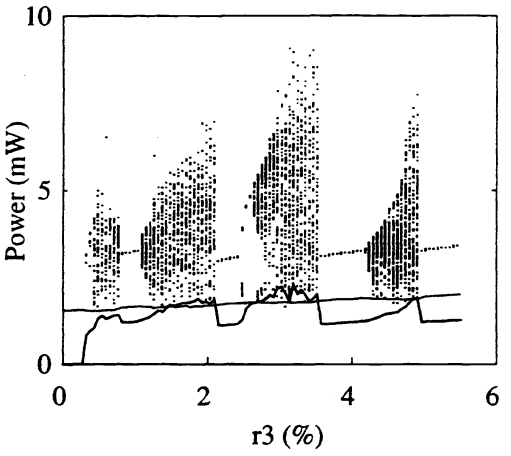

Figure 2 Bifurcation diagram (•••) of the laser power for L_{ext} = 10 cm as function of PCM field reflectivity for the ideal PCM (t_m = 0.0 ns). Also shown are the average power (-----) and the standard deviation of the power (——).

The PCM field reflectivity (r_3) relates to the feedback rate κ in Eqs. 2 and 9 as:

$$\kappa = \frac{(1 - r_2^2)}{\tau_{in}} \frac{r_3}{r_2} \tag{11}$$

where r_2 is the field reflectivity of the laser output facet and r_3 is the field reflectivity of the PCM. τ_{in} is the round trip time inside the laser.

Fig. 3 shows the same system but with a deep mirror, penetration time t_m = 0.1 ns. This deep PCM is relatively thin as compared to the relaxation oscillation period (T ~ 1/750 MHz ~ 1.3 ns). For low feedback levels ($r_3 \lesssim 3\%$), the bifurcation diagrams are similar. However, as the feedback level is increased above $r_3 > 4.5\%$, the deep mirror tends to suppress the chaos to the point that the laser becomes nearly stable for $r_3 > 5\%$. This is easily seen as the power standard deviation is nearly zero.

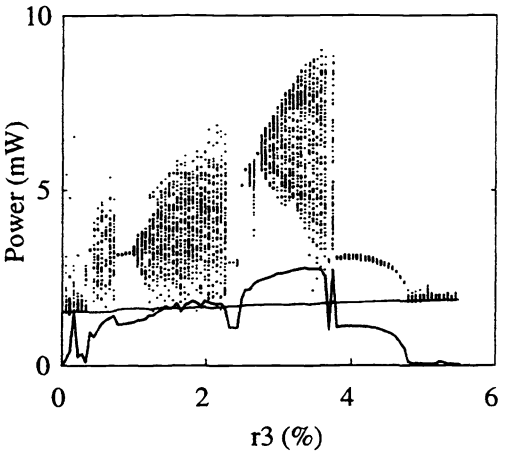

Figure 3 Same as Fig. 2 but $t_m = 0.1$ ns.

For Fig. 4, the depth of the mirror has been increased to $t_m = 0.4$ ns. This is now comparable to the relaxation-oscillation period (T ~ 1/750 MHz ~ 1.3 ns). There has been a great suppression of the chaos. In the range of $1.7\% < r_3 < 3.3\%$ the laser shows periodic behavior. For $r_3 > 3.3\%$ the laser operates stably.

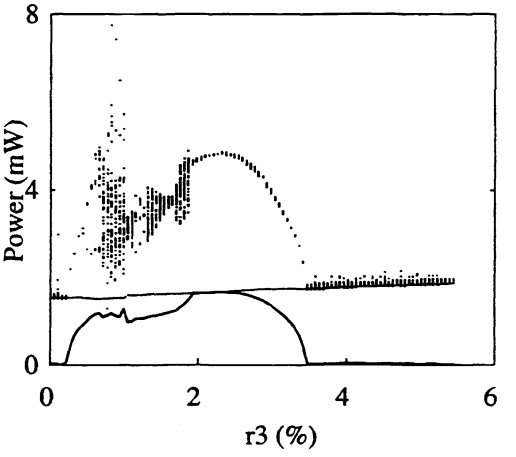

Figure 4 Same as Fig. 2 but $t_m = 0.4$ ns.

This behavior can be understood by inspection of Eq. 9. Basically, the integral performs a weighted averaging of the feedback. A greater t_m smooths the feedback more, leading to less chaos. Also, higher frequencies are attenuated more than lower frequencies, which would explain the tendency for period-one behavior for the deep mirror.

3.3 External cavity spacing

Changing the external cavity length can have profound effects on the dynamics of the laser system. For L_{ext} = 1, 10, 100 cm, Figs. 5, 2, and 6 respectively show that for the instantaneous PCM case, the changes in cavity length completely change the bifurcation diagrams. In general, as L_{ext} increases the chaotic regions become larger and there is less interruption by stable windows. This similar to ordinary feedback.[6]

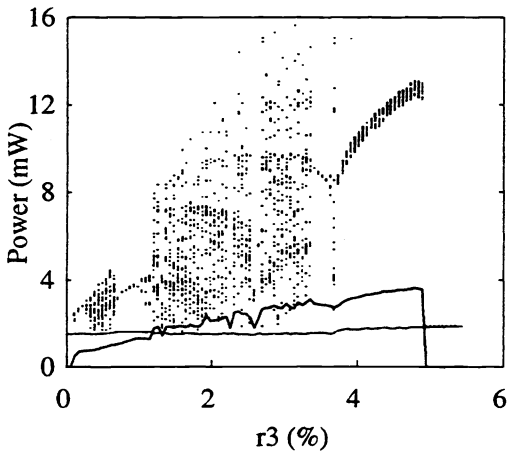

Figure 5 Same as Fig. 2 but L_{ext} = 1 cm.

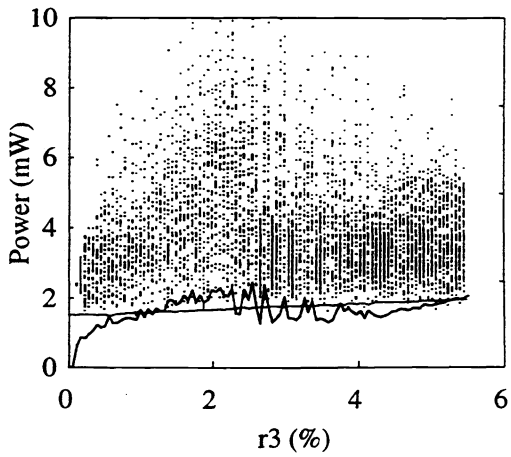

Figure 6 Same as Fig. 2 but L_{ext} = 100 cm.

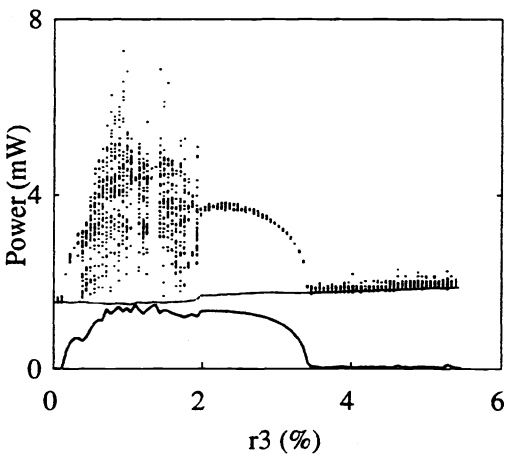

Figure 7 Same as Fig. 2 but t_m = 0.4 ns and L_{ext} = 1 cm.

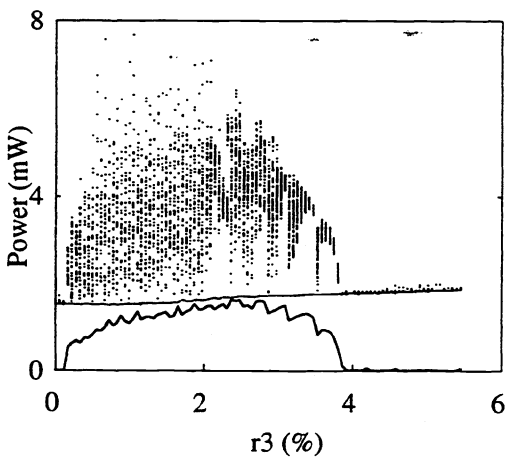

Figure 8 Same as Fig. 2 but t_m = 0.4 ns and L_{ext} = 100 cm.

The behavior with external-cavity length is less pronounced for the deep mirror, t_m = 0.4 ns. Figs. 7, 4, and 8 show, respectively, the bifurcation diagram for L_{ext} = 1, 10, and

100 cm. There is some tendency at weak feedback for there to be more chaos as L_{ext} is increased, but regardless of L_{ext}, the chaos always ends at about $r_3 \cong 4\%$, and the envelopes of the bifurcations points are similar. So while the external cavity length usually has a large effect on the laser dynamics, for the case of the deep mirror it is a secondary effect. The dynamics are dominated by the presence of the deep mirror. The instantaneous PCM dynamics tend to scale with $\kappa\tau$ (in other words, $r_3\tau$, where τ = external round trip time). The deep PCM dynamics tend to scale with just κ or r_3.

3.4 Current effects

Figs. 9 and 10 show the bifurcation diagrams for the instantaneous and deep PCM's, respectively, where I/I_{th} is the bifurcation variable. The average power values are identical, but once again the deep PCM shows a great suppression of chaos. Above about $I/I_{th} = 2.3$ the instantaneous case (Fig. 9) shows a large amplitude (note the σ is about 8 mW) period one oscillation that was damped out in the deep PCM case (Fig. 10). This is discussed more with the frequency effects in section 3.4.

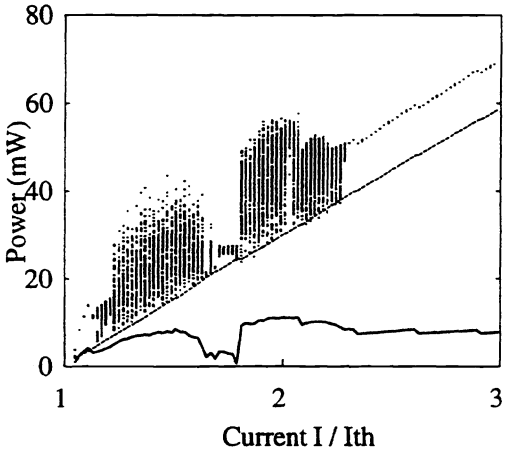

Figure 9 Similar to Fig. 2 except that current ratio I/I_{th} is now the bifurcation variable. $r_3 = 2.5\%$.

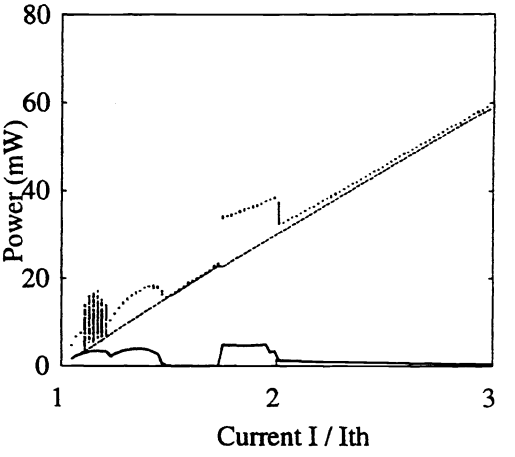

Figure 10 Same as Fig. 9 but $t_m = 0.4$ ns.

3.5 Tunable Frequency

A search for regions of pulsed operation can be tedious. A brute-force method such as viewing power verses time plots or doing Fourier transforms over a large parameter space is costly both in terms of human and computer time. However, the task is simplified by making use of the sampling performed in calculation of the bifurcation diagrams. The bifurcation diagrams are constructed by recording the value of P ($|E|^2$, photon number) whenever N crosses the N_{ave} plane in the direction of decreasing N. Thus for simple periodic behavior, the sampling of P will occur at nearly the same point in each cycle, and greater accuracy can be achieved by interpolating between the points of just before the N_{ave} plane and just after. Thus if we record

this sampling frequency, and compute its standard deviation (for little additional overhead), we can use this variable in conjunction with the standard deviation power bifurcation diagram to determine not only the presence of periodic behavior but also the frequency of oscillation. For example, for period-one behavior, the power bifurcation diagram yields a single line with a large standard deviation. The sampling variable frequency, however, gives the frequency of oscillation when its standard deviation is small. Below in Fig. 11 is a typical picture seen for regions of pulsed operation for the deep PCM, showing a frequency of 1.3 GHz. Note the power of the pulses goes all the way to zero.

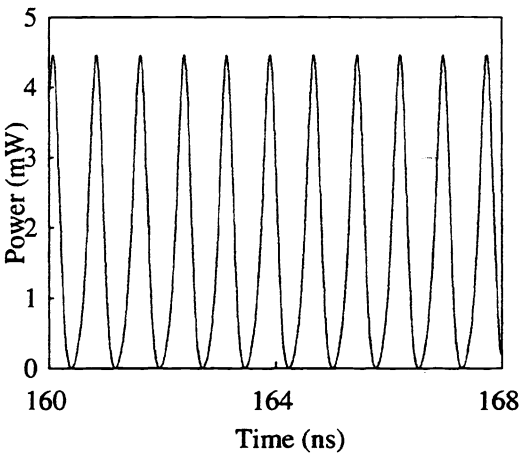

Figure 11 1.3 GHz pulsed operation.
$t_m = 0.4$ ns, $L_{ext} = 10$ cm, $r_3 = 2.48$ %.

Figs. 12 and 13 below show the sampling frequency verses feedback for an instantaneous PCM and a deep PCM, respectively. The instantaneous PCM tends to show regions of periodic behavior (small standard deviation of sampling frequency , and a line indicating period one behavior on the power bifurcation diagram, Fig. 2). The equal frequency spacing of 1.5 GHz (the external round-tip frequency) indicates a locking behavior between the relaxation oscillations and the round trip frequency ($1/\tau = 1.5$ GHz). Note that these frequency locking regions are absent for the deep PCM, Fig. 13, yet another indicator that the deep PCM is dominating the dynamics rather than the external cavity round trip frequency effects. Also, the instantaneous PCM shows much higher frequencies (about 1 to 6 GHz) than the deep PCM (about 1 to 1.5 GHz). As mentioned before, inspection of Eq. 9 shows that the deep PCM tends to filter out higher frequencies.

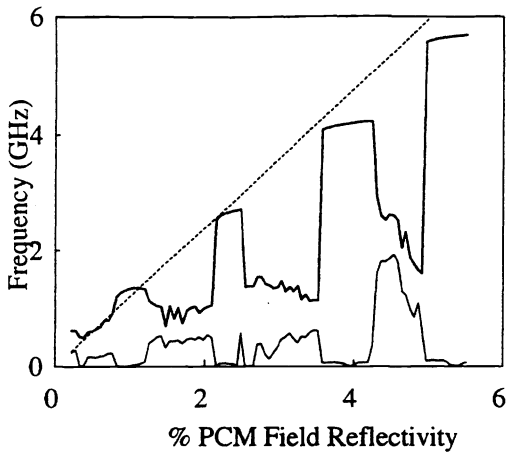

Figure 12 Average sampling frequency (—) as a function of feedback for t_m = 0.0 ns, L_{ext} = 10 cm, and r_3 = 2.48 %. Also shown are the σ_{freq} (——), and a theory fit (-----).

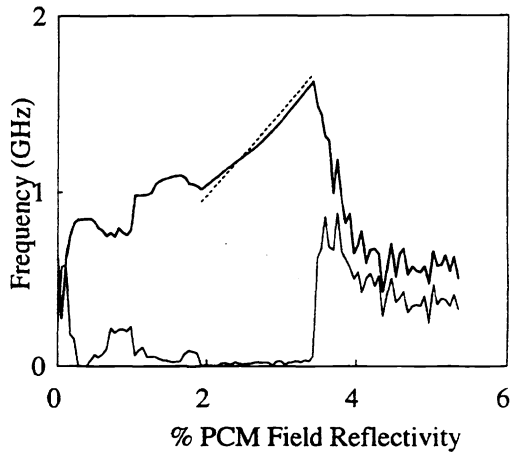

Figure 13 Same as Fig. 12 but t_m = 0.4 ns.

Both cases show linear frequency with r_3 behavior. This linearity can be demonstrated by assuming nearly stable operation with a small sinusoidal perturbation:

$$\begin{aligned} E &= E_{ave} + iE_1 e^{-i\omega t}\ ; \quad E_{ave} \gg E_1 \\ N &= N_{ave} + N_1 e^{-i\omega t}\ ; \quad N_{ave} \gg N_1 \end{aligned} \tag{12}$$

The i coefficient is due to the 90^0 phase shift between N and E. Plugging these into Eq. 2 and using a linear gain dependence on N ($G = G_N(N-N_0)$) yields:

$$\omega = \frac{E_{ave}}{E_1}\sqrt{(\kappa - G_0)^2 + (\alpha G_0)^2}\ ; \quad G_0 \equiv G_N(N_{ave} - N_0) - \gamma \tag{13}$$

For the case of low feedback $G_0 \approx 0$, so

$$\omega \cong \frac{E_{ave}}{E_1}\kappa \tag{14}$$

The result, which also occurs for deep PCF by plugging Eqs. 11 into Eq. 9, is plotted in Figs. 12 and 13. Even though the condition of a small oscillation is not held, surprisingly good agreement between this theory and the pulsed regions is evident.

For the case of bifurcation frequency verses current ratio I/I_{th}, similar behavior results.

For higher currents, $I/I_{th} > 2.3$, the instantaneous mirror (Figs. 9 and 14) once again shows locking plateaus spaced by the round-trip frequency of 1.5 GHz. This indicates locking behavior between the relaxation oscillation and round trip frequencies, absent for the deep PCM in Fig. 15. The plots are not shown, but this locking behavior was also absent for greatly different external round-trip frequencies (L_{ext} = 1 cm and L_{ext} = 100 cm).

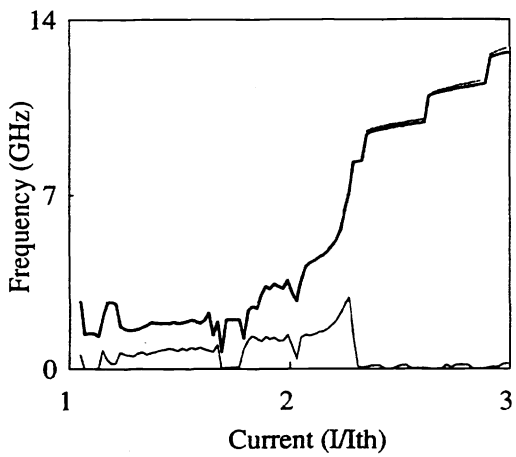

Figure 14 Average sampling frequency as a function of current (▬), σ_{freq} (——), and theory fit (-----). Parameters are t_m = 0.0 ns, L_{ext} = 10 cm, and r_3 = 2.48 %.

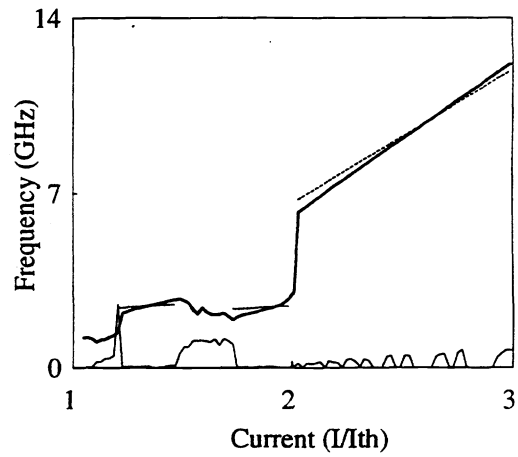

Figure 15 Same as Fig. 14 but t_m = 0.4 ns.

This apparently linear dependence of frequency on current was surprising, as the usual expression for a laser without feedback gives the relaxation oscillation frequency as $\omega \sim \sqrt{(I-I_{th})}$. Making analytical progress with the rate equations with feedback is difficult (hence the numerical integration!), however with some approximation this relation can be motivated. Taking the small amplitude oscillation approximation of Eq. 11 in Eq. 1 yields

$$\omega \cong \frac{1}{N_1}\left(\frac{I}{q} - \frac{N_{ave}}{\tau_e} - G_N (N_{ave} - N_0) E_{ave}^2\right) \tag{15}$$

By using a linear P verses I relation $E_{ave}^2 = \Gamma(I-I_{th})$ (where Γ is the slope of the LI curve), Eq. 15 becomes:

$$\omega \cong \frac{1}{N_1}\left(I\left(\frac{1}{q} - G_N \Gamma (N_{ave} - N_0)\right) + G_N \Gamma (N_{ave} - N_0) I_{th} - \frac{N_{ave}}{\tau_e}\right) \tag{16}$$

The ω verses I slopes from this equation were used in fitting the curves in Figs. 14 and 15. For higher currents ($I/I_{th} \geq 2$) the fits are good. As Eqs. 15 and 16 show, the I term would become more dominate for larger currents.

4. Conclusion

A model for phase conjugate feedback due to non-degenerate four-wave mixing has been derived. An efficient recursive definition was numerically implemented. It was found that the deep PCM tends to suppress chaos and higher frequencies, when the penetration time t_m becomes comparable to the relaxation oscillation period. Locking between the relaxation oscillation and the external round trip frequencies is absent with the deep PCM. It removes much of the external cavity spacing dependence in the laser dynamics. Regions with good pulses were found, with the frequency of the pulses being linearly tunable by varying the feedback level or the current. The presence of phase-conjugate feedback changes the frequency dependence of the relaxation oscillations for current from $\omega \sim \sqrt{I}$ to $\omega \sim I$.

Acknowledgements: Supported by a NATO Collaborative Research Grant, CRG 941327.

1. G. R. Gray, D. H. DeTienne, and G. P. Agrawal, "Mode locking in semiconductor lasers by phase-conjugate optical feedback," Optics Letters, **20**, pp. 1295-1297, June 1, 1995.

2. G. H. M. van Tartwijk, H. J. C. van der Linden, and D. Lenstra, "Theory of a diode laser with phase-conjugate feedback," Opt. Lett. **17**, pp. 1590-1592, Nov. 15, 1992.

3. S. Mailhot and N. McCarthy, "Influence of phase conjugate optical feedback on the emission properties of visible low-power diode lasers," Can. J. Phys., **71**, pp. 429-433, 1993.

4. T. Shimura, M. Tamura, and K. Kuroda, "Injection locking and mode switching of a diode laser with a double phase-conjugate mirror," Opt. Lett., **18**, pp. 1645-1647, 1993.

5. G. P. Agrawal and G. R. Gray, "Effect of phase-conjugate feedback on the noise characteristics of semiconductor lasers," Phys. Rev. A **46**, pp. 5890-5898, Nov. 1, 1992.

6. N. Cyr, M. Breton, M. Tetu, and S. Theriault, "Laser-diode frequency control by resonant phase-conjugate reflection from an atomic vapor," Opt. Lett. **16** pp. 1298-1300, Sep. 1991.

7. G. R. Gray, D. Huang, and G. P. Agrawal, "Chaotic dynamics of semiconductor lasers with phase-conjugate feedback," Phys. Rev. A **49**, 2096-2105, (1994).

8. D. M. Pepper and A. Yariv, *Optical Phase Conjugation*, ed. R. A. Fisher, Academic Press, 1983.

9. R. W. Boyd, *Nonlinear Optics*, Chap. 6, Academic Press, 1992.

10. J. Mörk, B. Tromborg, and J. Mark, IEEE J. Quantum Electron., **28**, p. 93, 1992.